On the simultaneous analysis of optical and thermal properties of thin films via pseudo-transmittance spectroscopy: aluminium nitride

2009 J. Phys. D: Appl. Phys. 42 055405

(http://iopscience.iop.org/0022-3727/42/5/055405)

IOP PUBLISHING JOURNAL OF PHYSICS D: APPLIED PHYSICS

J. Phys. D: Appl. Phys. **42** (2009) 055405 (11pp) doi:10.1088/0022-3727/42/5/055405

On the simultaneous analysis of optical and thermal properties of thin films via pseudo-transmittance spectroscopy: aluminium nitride

C García-Segundo[1,3], M Villagrán-Muniz[1] and S Muhl[2]

[1] CCADET de la Universidad Nacional Autónoma de México (UNAM). Circuito Exterior, Ciudad Universitaria, Apdo. Postal 70-186 CP 04510, DF, Mexico
[2] IIM de la Universidad Nacional Autónoma de Mexico (UNAM). Circuito Exterior, Ciudad Universitaria, Apdo. Postal 70-360 y 70-284, DF, Mexico
[3] State Key Laboratory of Magnetic Resonance and Atomic and Molecular Physics and Centre for Cold Atom Physics. Wuhan Institute of Physics and Mathematics, Chinese Academy of Sciences, Wuhan 430071, People's Republic of China

E-mail: crescencio.garcia@ccadet.unam.mx

Received 28 August 2008, in final form 1 December 2008
Published 12 February 2009
Online at stacks.iop.org/JPhysD/42/055405

Abstract
We present an experimental and theoretical method to simultaneously obtain the optical dispersion curves and the thermal properties of thin film samples. From the experimental and analytical perspectives, we establish the physical conditions to validate this novel approach. Similarly, the method is tested on thin films of aluminium nitride (AlN) deposited on quartz and crystalline silicon substrates. The experimental set-up is that used for the open photoacoustic cell pseudo-transmittance spectroscopy (OPC-PATS). The sample is illuminated with modulated light as a pre-condition to induce and detect photothermal waves. The amplitude of these waves is proportional to the optical absorption and to the thermal properties of the sample. This is displayed in the so-called pseudo-transmittance spectra that we report here. Theoretically, we extend a previously reported self-consistent method to provide, in addition to the refractive index and the extinction coefficient spectral curves, the ratio of the thermal to the optical transparency and the thermal conductivity. Although the current analysis is applied to the optical range, the conditions of the method are such that it can readily be extended to other wavelengths.

(Some figures in this article are in colour only in the electronic version)

1. Introduction

In solids and, in particular, for thin films, experimental analysis of optical properties and thermodynamic properties is carried out using separate methods. One finds that ellipsometry and photo-spectroscopy are often used in the former case, whilst thermo-mechanical and photoacoustic methods are used for the latter. However, from the literature [1, 2] it can be seen that there exists a certain overlap between these methods where a given technique generates acoustic-like waves by a process of optical absorption. When these acoustic-like waves are at low frequency they can be detected using an open photoacoustic cell (OPC) transducer. Additionally, if these waves are produced and detected as a function of the wavelength of the pump light, one can perform spectroscopic analysis. In particular, when these spectra are produced in a transmittance-like configuration, as shown in figure 1, one performs photoacoustic pseudo-transmittance spectroscopy (PATS). It has been shown for thin films [1] that the obtained spectra are quite similar to the conventional optical absorption spectra, and even though the raw data are not optical one can directly determine the optical properties of dielectric thin films.

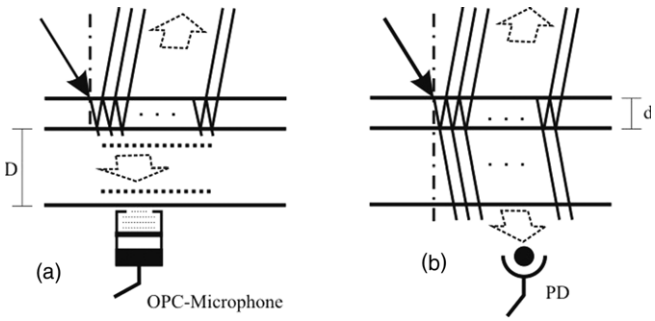

Figure 1. The sample is of a thin film of thickness d on an opaque substrate of thickness D; the figures illustrate the schematic configurations for (a) pseudo-transmittance PATS, where the output signal is registered via an OPC-microphone, and (b) the optical transmittance, where PD is an optical sensor, such as a photodiode.

On the other hand, the process of generation and interpretation of these acoustic-like waves has been widely studied and applied to the study of gases and condensed media [2–4]. One common application is to perform absorption spectroscopy to monitor chemical and structural changes or to accurately measure the thermal diffusivities of solids or gases [5, 6]. There also exists the so-called OPC-spectroscopy, which has been applied to the thermal characterization of thick-layered structures [7]. However, as far as we know from the literature, no attempt has been made to obtain simultaneously the optical and thermal properties of a single sample.

The main goal of this paper is to display that it is possible to derive the optical and thermal properties of dielectric thin films at the same time. We indicate that this capability results from (1) the physical rules and principles involved in the signal generation, (2) the conversion of incident energy in terms of optical to thermo-mechanical, (3) the transport of the resulting energy burst as an acoustic-like wave and (4) that the output data will contain both the optical and the thermal information, relative to the tested sample [2].

1.1. General background

When light is incident on a macroscopic solid a certain fraction is absorbed and *converted* into thermo-mechanical energy. Eventually this diffuses and dissipates within the bulk of the sample; this is labelled as non-radiative energy since it evolves from non-radiative processes and this process is adequately described by transport theory [3–5]. The efficiency of this energy conversion (also known as caloric efficiency) is determined by the optical properties of the sample together with its thermal properties. By means of illuminating a sample with modulated light at an appropriate frequency [3, 6] it is possible to obtain an output of these non-radiative processes in the form of a sound-like wave: a photothermal wave. Similarly, if the sample is illuminated on one side with a range of wavelengths and the photoacoustic output is detected at the opposite side as a function of the illumination wavelength, then this is the so-called photoacoustic (PA) spectrum. For the configuration we described this spectrum is a function of the sample's optical transmittance and this method is the photoacoustic pseudo-transmittance spectroscopy (or PATS).

In this paper, we analyse the general physical properties of the data obtained from PATS using an open photoacoustic cell, or OPC-PATS, and we describe a way to deduce the optical and thermodynamic diffusive properties of thin films on transparent and opaque substrates studied using this technique. As in [1], we have tested our procedure on data obtained from AlN thin film samples deposited on quartz darkened with carbon black and on crystalline silicon.

The required parts necessary to achieve our objective are: (1) to derive a set of equations for the interpretation of the experimental data and thus derive the optical and thermal properties of a given sample and (2) to establish that the OPC-PATS technique produces reliable data, related to the optical and the thermal properties of such a sample, in a simultaneous way.

2. Theory

The configuration we consider to produce and detect the photothermal waves, in transmittance, is displayed in figure 1(a). For clarification, we show in figure 1(b) for comparison the schematic of the conventional configuration for optical transmittance. We assumed that the thin film, of thickness d, was deposited on a thick opaque substrate of thickness D, such that $D \gg d$. Additionally, with the aim of broadly validating our approach we consider that the same thin film was deposited on two types of substrate: (1) pieces of quartz that were made optically opaque by painting the surface opposite the thin film with carbon black and (2) substrates of crystalline silicon, which are optically opaque and therefore do not require any particular preparation.

Since the experimental output is in the form of thermo-mechanical waves similar to sound waves, a membrane microphone was used as shown in figure 1(a). From figures 1(a) and (b) it is clear that the amplitude, H, of the output signal is proportional to the transmittance of the sample and therefore to the energy conversion efficiency (assuming that the reflectance and scattering do not vary with wavelength). The incident light beam should be modulated at a sufficiently low frequency ($10\,\mathrm{Hz} < f < 100\,\mathrm{Hz}$) [2, 3, 6] such that the thermal properties of the top layer are determined without the contributions from the other layers. The modulation frequency defines how the absorbed energy diffuses within the sample. This is because the thermal diffusion coefficient, $\sigma = (\pi f/a)^{1/2}$, depends on the modulation frequency and the thermal diffusivity $a = \kappa/\rho c$, where κ is the thermal conductivity, ρ is the density and c the specific heat at constant pressure [2, 6]. For this work the modulation frequency was $f \cong 15\,\mathrm{Hz}$; the details of this choice and on how the modulation frequency affects the amplitude H can be found in the literature [1–6].

This frequency choice will be seen to have some consequences when we compare the value of σ with the coefficient of optical absorption, α_0, also expressed in cm^{-1}. The reciprocal of these parameters gives the characteristic optical thickness (optical attenuation or optical length, $\mu_\alpha = 1/a_0$) and the characteristic thermal thickness

Table 1. Any given material can be optically thin or thick. Each possibility shall exhibit up to three variants of thermal thickness; these determined by its thermal properties.

Transparent (optically thin) $\mu_\alpha > 1$	Thermally thin $\mu_\sigma \gg l$	Thermally thin $\mu_\sigma > l$	Thermally thick $\mu_\sigma < l$
Opaque (optically thick) $\mu_\alpha < 1$	Thermally thin $\mu_\sigma \gg l$	Thermally thick $\mu_\sigma < l$	Thermally thick $\mu_\sigma \ll l$

(thermal attenuation or thermal diffusion length, $\mu_\sigma = 1/\sigma$), respectively.

The general model and the theory that describes the sound-like waves and their interpretation through OPC detection can be found elsewhere in the literature [3, 4, 6]. The overall result of the theory is a *master* equation that can be simplified depending on how the two characteristic lengths compare. Therefore, as a starting point we reproduced this equation as follows (the details of its deduction can be found in [3, 4, 6]).

$$H = \frac{G}{\Lambda}\frac{I_0}{\kappa\sigma}\frac{r}{r^2-1}\frac{2r - \mathrm{e}^{-\alpha_0 d}[(r+1)\mathrm{e}^{\sigma d} + (r-1)\mathrm{e}^{-\sigma d}]}{[\mathrm{e}^{\sigma d} - \mathrm{e}^{-\sigma d}]}. \tag{1}$$

This is the analytic representation of the measured amplitude of H, which represents the rate of change in local temperature due to the non-radiative processes triggered by the modulated illumination. It includes terms related to (1) the sample and environment, which remain constant over the experiment (temperature, humidity, etc) and represented by G; and (2) the instrument contributions (Λ), which also remain constant over the experiment. The variable r represents the ratio between the optical absorption and the thermal diffusion coefficient: $r = \alpha_0/\sigma$. This ratio can also be interpreted as a measure of the dominance of the thermal or optical phenomenon. For the present case the parameters G and Λ are taken as constants since they are related to instrumental factors. For convenience we define $G/\Lambda \equiv \Xi$.

Equation (1) is simplified in a number of cases depending on the relative values of the thermal and optical lengths, where these are considered as boundary conditions. These cases are listed in table 1. Therefore, the main task is to obtain the equation(s) for each case in the combination of boundary conditions and thus derive a method from which we can quantify the optical and thermal properties for thin films, without the influence from the substrate.

Explicitly, for a given material of thickness d, it is optically opaque (or optically thick) if $\mu_\alpha < 1$ and it is (1) thermally thin if $\mu_\sigma \gg d$; or (2) thermally thick if $\mu_\sigma < d$ or $\mu_\sigma \ll d$. Conversely, it is optically transparent (or optically thin) if $\mu_\alpha > 1$ and it is (1) thermally thick if $\mu_\sigma < d$ or (2) thermally thin if $\mu_\sigma > d$ or if $\mu_\sigma \gg d$.

Using equation (1) we derive equations for these cases. The first case is of the optically thick material. The transmittance is $T = \exp(-\alpha_0 d) \approx 0$, and yet it can be

(a) Thermally thin: $\mu_\sigma \gg d$; then $|r| \gg 1$ and therefore $\mathrm{e}^{\pm\sigma d} \approx 1$, resulting in

$$H = \Xi\frac{I_0}{\sigma\kappa}\frac{1}{\sinh(\sigma d)}. \tag{2a}$$

(b) Thermally thick: $\mu_\sigma < d$; then $|r| > 1$, and $\mathrm{e}^{-\sigma d} \approx 0$, giving

$$H = \Xi\frac{I_0}{\sigma\kappa}\frac{\mathrm{e}^{\sigma d}}{\sinh(\sigma d)}. \tag{2b}$$

(c) Thermally thick: $\mu_\sigma \ll d$; then $|r| < 1$, and again $\mathrm{e}^{-\sigma d} \approx 0$. Thus equation (2*b*) also applies to this case.

As a result, for optically thick materials, we concluded that the output signal has no dependence on the optical properties and can be treated by means of the elasto-mechanic theory alone. Moreover, even though an optical beam is used to trigger the wave signal the result is a thermoelastic wave; i.e. it loses its optical character.

The other set of cases to analyse is that of an optically thin material. This has a transmittance $T = \exp(-\alpha_0 d) \neq 0$, meaning that H will depend on the optical properties of the material. An optically thin material can also be

(a) Thermally thin: $\mu_\sigma \gg d$; then $|r| > 1$, and $\mathrm{e}^{\pm\sigma d} \approx 1$. Therefore equation (1) is reduced to

$$H = \Xi\frac{I_0}{\sigma\kappa}\xi\frac{1}{\sinh(\sigma d)}(1 - \mathrm{e}^{-\alpha_0 d}). \tag{3a}$$

(b) Thermally thin: $\mu_\sigma > d$; this time $|r| < 1$ and $\mathrm{e}^{\pm\sigma d} \approx 1 \pm \sigma d$, resulting in

$$H = \Xi\frac{I_0}{\sigma\kappa}\xi\frac{1}{\sinh(\sigma d)}\left(r - \frac{\mathrm{e}^{-\alpha_0 d}}{r}\right). \tag{3b}$$

This case needs to be treated with care given the dependence on the actual thickness of the sample. For instance, a particular situation that can occur is when $r = \alpha_0/\sigma \approx 1$, with the result that the respective equation would have the same form as equation (3*a*).

(c) Thermally thick: $\mu_\sigma < d$; $|r| \ll 1$, and straightforwardly $\mathrm{e}^{-\sigma d} \approx 0$. Thus

$$H = \Xi\frac{I_0}{\sigma\kappa}r\mathrm{e}^{-\alpha_0 d}. \tag{3c}$$

In each of these equations, as specified, κ is the thermal conductivity, d is the respective layer thickness and $\xi = r^2/(1-r^2)$. It should be noted that the initial system of six cases is reduced to four equations.

The layered system as dealt with here is displayed in figure 2(*a*), and an example of the possible generalization is displayed in figure 2(*b*). The component layers in this system are represented by equations (2*a*), (2*b*), (3*a*), (3*b*) and (3*c*), as we describe later, in which the modulation frequency is already included within Ξ (see [1, 7] for details).

To clearly understand the relationships between the thermal and optical processes it is necessary to analyse the

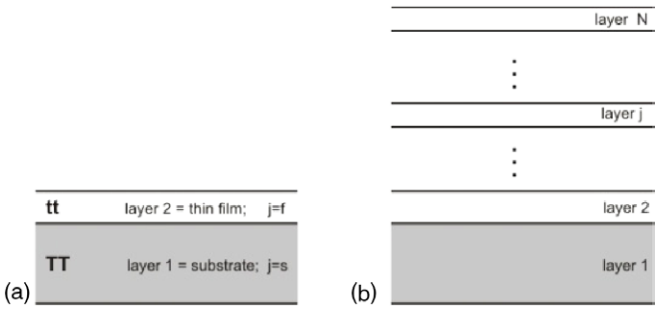

Figure 2. (*a*) A schematic of the system as described in the main text. This is a two-layer system where the thin film is optically transparent and thermally thin. However, we also consider two kinds of substrate that are optically thick, with one thermally thin and the other thermally thick. This suggests that equations (2*a*) and (2*b*) could be set in a modular way to analyse structures as complex as that shown in (*b*) with N layers and $N > 2$.

various times involved between the arrival of the light and its detection as an acoustic wave. This analysis is within the various relevant time frames [4, 5] as we describe next: (1) τ_o is the time for the non-radiative wave generation, this is the time clock from the instant of arrival of the modulated light up to the generation of the non-radiative burst, H, inside the sample. (2) $\tau_L = d_j/c_j$ is the time it takes for the light to travel through to the jth layer, where c_j is the speed of light in a medium j of thickness d_j. (3) $\tau_s = d/v_s$ is the time scale within which the non-radiative wave travels through the complete thickness d of the sample at the sound speed v_s. This distance is measured from the point of generation of the non-radiative wave up to the detection point. In the samples that we consider $d \leqslant \lambda$, and therefore these time scales compare as follows: $\tau_0 \gg \tau_L$ and $\tau_0 \approx \tau_s$. Additionally, since we are using low modulation frequencies (15 Hz), one can consider that within the τ_o time scale the beam of light interacts with the thin films and the substrate, simultaneously.

From equations (2*a*), (2*b*), (3*a*), (3*b*) and (3*c*) it is clear that the magnitude of the response from each layer (H_j) depends on the arriving intensity of the modulated beam of light. As the light beam travels across the layers, the optical dispersion theory predicts that the local relative intensity will be modulated by the transmittance (T_j) of the preceding layer(s). Therefore, the structure naturally imposes that, sequentially, each layer produces a response to the impulse $H_j \propto T_{j-1} I_{1-j}$, whose magnitude depends on the preceding optical transmittance and its own energy conversion efficiency (related to its thermo-mechanical properties). Therefore we suggest that the total effective non-radiative output can be given by the product of each individual response to the impulse: $H = H_1 H_2 \cdots H_j \cdots H_N$. With this we establish that in this system, each burst (photothermal wave) is composed of a given collection of sequentially well-defined responses that can be represented in terms of its frequency. It should be made clear that this assumption cannot be extended to thick layers because $d \gg \lambda$, resulting in $\tau_o \ll \tau_s$. The interested reader can check references [2–7], where many of these cases are considered along with the descriptions on how to construct the corresponding effective output signals.

For the case of two consecutive layers a possible complication could be the generation of a shared stress or a back-thermal response, from the transverse thermal expansion or temperature gradient across the thickness of the sample [2, 7]. However, if this does occur it will be of quite a small magnitude along the transmittance direction and we consider that it would not alter significantly the signals we are describing. Therefore, we assume that any interface contribution that causes signal broadening or damping of the transport or detection process is small enough and can be neglected.

Therefore, for the system shown in figure 2(*a*), according to the previous description we can expect that at the back face of the substrate, opposite to the incident light, the output signal will be composed of a sequence of two independent sets of responses to the incident impulse; with these being overlapped in space and time. Implicitly in the detection process these sets will be integrated. The response to the impulse is in the frequency domain (signal generation), followed by its Fourier transformation to the amplitude domain (signal detection). This is nothing else but the convolution of the signals: those generated by the thin film with the one generated by the substrate. Therefore, the effective total output is the product of the amplitudes from the thin film and that from the substrate, both modulated by the appropriate optical transmittance as represented by equations (2*a*), (2*b*), (3*a*), (3*b*) and (3*c*). This is multiplied by a 'constant' factor that accounts for the initial source intensity and its spectral distribution at a given point, i.e. the contributions from the experimental set-up and the environment. The quotes are to explicitly accept that this is not a true constant but will be constant for a given set of experimental conditions. Furthermore, as described in the next section, it is possible to obtain the output signal free from these contributions.

Experimentally, using a lock-in amplifier to detect the signal amplitude and the phase difference between sequential contributions it would be possible to get the output signal in the frequency domain, as superposed spectra. However, such a representation of the output is difficult to analyse. Instead, even though transducer devices are not perfect integrators (various frequencies are filtered) as indicated in [5–7], the OPC-filtering effects are of little importance and therefore the amplitude representation is the best option. For a particular sample it is necessary to define the boundary conditions and then choose the corresponding equations (2*a*), (2*b*), (3*a*), (3*b*) and (3*c*) to carry out the analytic representation.

Using the thermal diffusion coefficient defined as $\sigma = (\pi f/a)^{1/2}$, for $f = 15$ Hz and the thermal diffusivity of AlN being $\alpha_{AlN} = 1.47\,\mathrm{cm^2\,s^{-1}}$ [9], we then obtain $\mu_{\sigma AlN} = 1.766$ mm ($\mu_{\sigma AlN}$ is simply a particular value $\mu_{\sigma F}$). From ellipsometry measurements at 632.8 nm wavelength, we know that all the samples analysed had a thin film thickness (d_F) of around 0.5 μm, i.e. $\mu_{\sigma F} \gg d_F$. This corresponds to the case of a thin film that is optically transparent and thermally thin whose output signal can be represented by equation (3*a*).

For the films deposited on transparent quartz, if the transmitted light were allowed to reach the transducer structure this would trigger a signal that would mask the output from the

sample. To overcome this complication the back surface of the substrate was coated with a thick layer of matt carbon black. This blocks the light from reaching the detector and at the same time acts as a black body reference; its caloric efficiency is assumed to be equal to one. This was validated in a set of results reported in [1]. The same work also demonstrated that the quartz did not contribute to the output, the substrate contributions are those from the carbon black alone and this layer is optically thick and thermally thin.

The second type of substrate was crystalline silicon. Naturally this is optically thick, with $a = 0.68\,\mathrm{cm^2\,s^{-1}}$ [10], thus at 15 Hz we get $\mu_\sigma = 1.085\,\mathrm{mm}$, making $\mu_\sigma \gg d_{\mathrm{Si}}$ ($\cong 0.5\,\mathrm{mm}$), indicating that the output signal can be described by equation (2*a*).

The total (H_{T}) output (thin film and substrate) is given by $H_{\mathrm{T}} = H_{\mathrm{F}} \cdot T_{\mathrm{F}} \cdot H_{\mathrm{S}}$, where $T_{\mathrm{F}} = \exp(-\alpha_{0\mathrm{F}} d_{\mathrm{F}})$ is the optical transmittance of the thin film. As in transmittance optical spectroscopy, to remove the substrate effects it is necessary to acquire a reference baseline of the substrate alone, $H = H_{\mathrm{S}}$. Then, by simply taking the ratio $H_{\mathrm{T}}/H_{\mathrm{S}} = H_{\mathrm{F}} T_{\mathrm{F}}$, it is possible to obtain the thin film spectrum free from contributions related to the experimental set-up, the environment and the substrate.

In equation (3*a*), the term in brackets represents the optical absorbance, which in a first order approximation can be expressed as $1 - \exp(-\alpha_{0\mathrm{F}} d_{\mathrm{F}}) \cong 1 - (1 - \alpha_{0\mathrm{F}} d_{\mathrm{F}}) = \alpha_{0\mathrm{F}} d_{\mathrm{F}}$. Therefore, assuming the case of a single AlN thin film system and after applying this approximation to (3*a*), one finds that the expression representing the experimental PATS data is

$$\Theta = \left(\frac{\alpha_{0\mathrm{F}}^2}{\sigma_{\mathrm{F}}^2 - \alpha_{0\mathrm{F}}^2}\right) \frac{\alpha_{0\mathrm{F}} d_{\mathrm{F}} T_{\mathrm{F}}}{\sigma_{\mathrm{F}} \kappa_{\mathrm{F}} \sinh(\sigma_{\mathrm{F}} d_{\mathrm{F}})}. \tag{4}$$

Equation (4) expresses the central idea of the analysis we present in the rest of the paper and therefore we wish to carefully evaluate it to gain a better insight into its implications. We can see that both $\alpha_{0\mathrm{F}}$ and σ_{F} are in units of $\mathrm{cm^{-1}}$; consequently in (4) the ratio $\alpha_{0\mathrm{F}}^2/(\sigma_{\mathrm{F}}^2 - \alpha_{0\mathrm{F}}^2)$, defined earlier as ξ_{F}, is an adimensional number. We also note that the remaining part of (4) exhibits a linear relationship of Θ with the film's optical parameters and an inverse relation with its thermal parameters. However, a dimensional analysis shows that Θ, as expressed in (4), has units of temperature divided by power density. In other words, Θ represents the rate of change of the temperature in the sample due to the flux of optical power per unit of area.

This aspect helps support the idea that the method can be used to determine the optical properties of thin films, as presented in [1], and the thermal properties of a thin film starting from the very same set of experimental data, as we present this time.

Now, in relation to the structure of the PATS spectra, these are made up of two parts: (1) a basic trend which depends on the complex refractive index of the thin film and on top of this are the effects due to optical interference, (2) the interference fringes, the period of which depends on the thin film thickness whilst the position of the maxima and the minima depends on the angle of incidence of the illumination. However, the general attributes are defined by the optical dispersion properties [11]. This was verified in [1] and used to construct a general method to obtain the value of the refractive index of the thin film as a function of wavelength.

The optical absorbance, as defined by Beer's law, is $\alpha_0 = -\ln(T)/d$, while from optical dispersion theory it is $\alpha_0 = 4\pi\kappa/\lambda$ [11, 13]. Therefore, from the PATS data, which in the present description are represented by Θ we can obtain both the transmittance and the absorbance of the film, T_{F} and $\alpha_{0\mathrm{F}}$, without considering the thermal information that is also contained in the data. It should be noted that in the derivation of equation (4) one of the boundary conditions is that $d\sigma_{\mathrm{F}} \ll 1$. Therefore, without loss of generality, this equation can be further simplified by taking $\sinh(\sigma_{\mathrm{F}} d) \approx \sigma_{\mathrm{F}} d$, and since $\xi_{\mathrm{F}} = r^2/(1 - r^2) = \alpha_0^2/(\sigma^2 - \alpha_0^2)$, we can rearrange terms in equation (4) to get

$$\sigma^4 - \alpha_0^2 \sigma^2 - \frac{\alpha_0^3 T}{\kappa \Theta} = 0. \tag{5}$$

We have removed the F-suffix for ease of presentation. Let us assume that σ is a known parameter. Then we solve for the thermal conductivity to obtain

$$\kappa = \frac{\alpha_0^3}{(\sigma^2 - \alpha_0^2)\sigma^2} \frac{T}{\Theta}. \tag{6}$$

The thermal conductivity is explicitly set in terms of the optical absorption, the thermal diffusion coefficient and the ratio of optical transmittance to pseudo-transmittance (as defined in (4)). Note that (6) has no dependence on the sample's thickness, as expected for any thermal conductivity expression. This represents the variation of the thermal conductivity with the optical absorption, as a function of the wavelength of illumination. The optical absorption value can be seen as a measure of coupling of the external field with the solid as a function of the wavelength. The transference (coupling) of the absorbed energy to thermal energy will appear in terms of a phonon distribution with different efficiency transference for each wavelength. Thus one can take (6) as a measure of the thermal conductivity variation, related to this phonon distribution within the experimental range. After all, the thermal conductivity is directly related to the phonon mean-free-path (heat-carriers-free-path), which is determined by phonon–phonon scattering.

On a different path-line of this analysis we assume κ as known parameter, and then from (5) we can derive an explicit expression for σ. We take (5) as a four degree equation, and we find that it has two real solutions (one is the negative of the other) and two complex solutions; as shown next

$$\sigma = \pm \frac{\alpha_0 \sqrt{1 \pm \sqrt{1 + 4(T/\Theta)(1/\kappa\alpha_0)}}}{\sqrt{2}}. \tag{7}$$

Since σ can be real or complex and since all the involved parameters are positive, we only get meaningful solutions using the outermost positive sign in equation (7). The solution with the additive inner square root produces the real and positive solution, while the subtractive case produces the complex and positive solution. By rearranging (7) we can get an expression for the inverse of the ratio r. Now we know

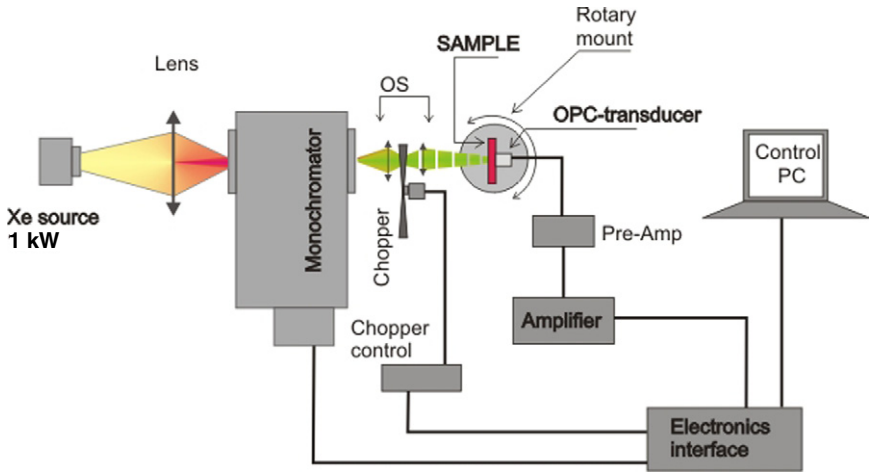

Figure 3. Experimental set-up, the sample was firmly attached to the OPC-transducer, clamped to a rotary mount. This permitted spectra to be taken at different angles of illumination. The OS is an optical telescopic system used to focus the output of the monochromator.

that $0 < 4T/(\Theta\kappa\alpha_0) < 1$; therefore, the innermost square root should always be positive and also always bigger than one. Moreover, from the initial conditions we have $|r| > 1$, and thus $1/|r| < 1$; therefore the only meaningful solution is

$$\frac{1}{r} = \frac{\sigma}{\alpha_0} = \frac{1}{\sqrt{2}}\sqrt{1 - \sqrt{1 + 4\frac{T}{\Theta}\frac{1}{\kappa\alpha_0}}}. \tag{8}$$

Therefore we have recovered $|r|$ which, from the boundary conditions imposed to obtain equation (3*a*), is positive and real. For simplicity, we have not included thermal dissipation processes in this model [3–5]. There are a number of works [1–7] that support this exclusion.

The significance of (8), the optical thickness to thermal thickness ratio, is to explicitly display that the coupling of optical energy with the thermal energy depends on two physical properties: the optical absorption and the thermal conductivity; appearing there as the product $\alpha_0\kappa$. Thus, from (6) or from rolling back (8), after recognizing that each term is real and positive, it turns out that this product is expressed as

$$\kappa\alpha = \frac{T}{\Theta}\left(\frac{r^4}{1 - r^2}\right). \tag{9}$$

Here one recognizes that for a given sample $|r|$ is a constant, and it will remain like that unless a chemical change occurs. Therefore in (9), this time for an optically thin and thermally thin material, the term in brackets will define a constant trajectory with negative slope (since $|r| > 1$). Clearly, the present results cannot cover cases where the boundary conditions are different from the current ones; these cases would require separate analysis.

3. Experiment

The AlN films were deposited on quartz and pieces of crystalline silicon wafer by dc magnetron reactive sputtering as described in our earlier paper [1]. The samples were placed in the experimental set-up for the acquisition of the pseudo-transmittance spectra using illumination at 0° and 50° with respect to the normal to the sample solidly mounted on the OPC-transducer. The set-up is shown in figure 3, and the details can be found in [1]. The light source was a 1 (one) kW Xe^+ halogen arch lamp projected to illuminate the 1200 lines $inch^{-1}$ grating of a monochromator. The output from the monochromator was reduced to illuminate a $2 \times 3\ mm^2$ area of the sample and chopped at 15 Hz frequency. The chopper also provides the reference signal for the lock-in amplifier used to synchronize the data acquisition. The set-up is isolated from radiant infrared components and from acoustic noise. The samples were placed in the experiment such that illumination and signal output were as schematically represented in figure 1(*a*). The thin film sample on quartz was darkened with matt-black-carbon on the side opposite to the illuminated surface; in this way the light was prevented from arriving at the sensing microphone. For this case, we also took a spectrum of the darkened piece of quartz without a film and this was used for normalizing the spectra (removing the substrate contributions).

The AlN samples were also measured using ellipsometry at 632.8 nm to obtain the refractive index and film thickness, 590 nm and 530 nm for the quartz and crystalline silicon substrates, respectively. The refractive index of the film on the quartz substrate was 2.1 ± 0.06 but for the crystalline silicon it was not possible to establish a precise value. The cause of this complication was later explained by the PATS analysis and confirmed through Rutherford backscattering analysis (RBS) as described in the next section.

A recording of each substrate alone at the corresponding incidence angle was made immediately after each spectroscopic recording of the thin film/substrate system. This curve was used as the baseline or reference spectrum. In figure 4 we display examples of these curves. The top curve is of AlN on crystalline silicon, the middle curve is from the crystalline silicon alone and the bottom curve is the quartz substrate coated with the carbon black.

4. Results of the optical and RBS analysis

4.1. Optical analysis

For each angle of incidence, each film/substrate spectrum was divided by its corresponding baseline spectrum and each of the resulting spectra were analysed using the self-consistent method described in the previous section. We used ellipsometry to obtain a first estimate: (1) of the film thickness, 569.0±30 nm, and (2) of the refractive index at the wavelength of the measurement (632.8 nm), 2.02 ± 0.15. These values were compared with estimates calculated from the induced spectral shift in the interference figures. For the thickness the estimate was performed using

$$d = \frac{1}{2}\left[\frac{A^2 - B^2}{\sin^2\theta_{02} - \sin^2\theta_{01}}\right]^{1/2} \tag{10}$$

and for the refractive index,

$$n = \left[\frac{(A\sin\theta_{02})^2 - (B\sin\theta_{01})^2}{A^2 - B^2}\right]^{1/2}. \tag{11}$$

These are equations (5) and (6) reported in [1]. Here $A = (\lambda_{11}\lambda_{12})/\Delta\lambda_1$ and $B = (\lambda_{21}\lambda_{22})/\Delta\lambda_2$, and $\Delta\lambda_1 = \lambda_{11} - \lambda_{12}$ and $\Delta\lambda_2 = \lambda_{21} - \lambda_{22}$ are the shift of the spectra maxima for the two angles of incidence, θ_{01} and θ_{02}. In these equations, d and n are independent variables which depend only on the optical characteristics.

After applying the method reported in [1], we derive the data for the refractive index and the optical attenuation of AlN as a function of wavelength within the experimental range. In figure 5 we display the obtained curves for AlN on quartz; the top curve is the refractive index as reported in [1], which is comparable to that reported by Brunner *et al* [14]. The lower curve is the optical attenuation for AlN, which is relevant for the thermal analysis.

By applying equation (10) to the data we find that the thickness is 264.91 ± 25 nm. From (11) we obtain that for a wavelength of 633 nm the refractive index is 2.134 ± 0.13. The thickness estimate is in clear disagreement with the single wavelength ellipsometry measurements; this point will be discussed extensively later.

Figure 6 shows the refractive index and optical attenuation for the crystalline silicon substrate sample. The forms of the curves are similar to those obtained for the quartz sample except that they have larger values.

The experimental conditions for the deposition of the films on the quartz and crystalline silicon substrates were the same

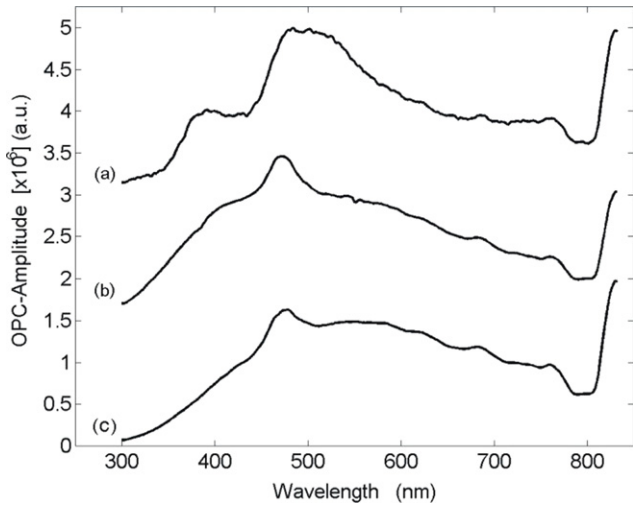

Figure 4. Digital representation of the raw curves obtained from the experimental set-up. Curve (a) is for AlN on crystalline silicon, curve (b) is from the crystalline silicon alone, and curve (c) is for bare quartz with matt-black-carbon on the side opposite to the illuminated surface. The relative scale shifting is for the purpose of clarity only.

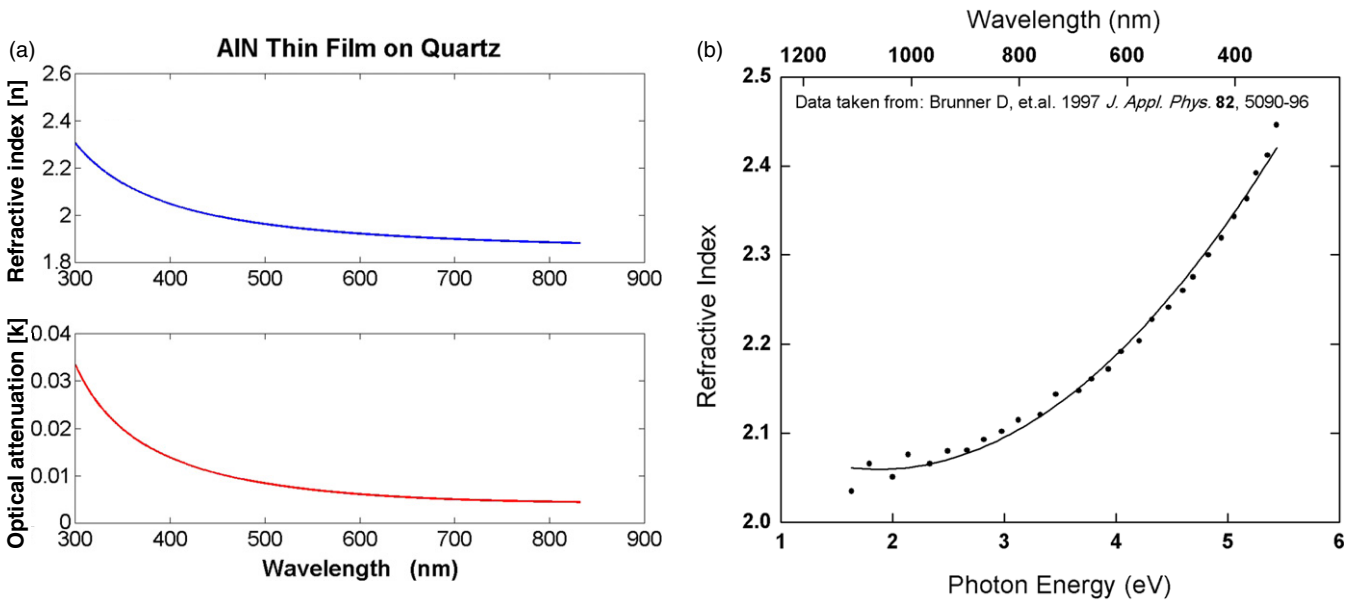

Figure 5. In (*a*), the top curve is the refractive index of AlN on quartz, while the bottom one is the optical attenuation. Both were directly obtained from the PATS curves. (*b*) This curve is from data taken from Brunner *et al* [14], and reproduced here for comparison purposes.

and therefore it was surprising that the results for the two substrates were significantly different. In order to obtain an independent characterization of the thin films and the film–substrate interface we carried out RBS of the samples.

4.2. RBS analysis

For this analysis we used a 960 keV deuterium beam perpendicularly incident to the sample. Both the elastic and the nuclear reaction (NR) particles produced by the deuteron bombardment were detected by the surface barrier detector placed at 165° relative to the incident deuterium beam. With this arrangement we obtained the density per area unit and the composition of the AlN film as well as the thickness and composition of the film–substrate interface layer. A detailed analysis of the RBS data showed that the interface layer consisted of a mix of silicon oxide and silicon oxinitride with an approximate thickness of 150 nm [13]. This layer was not considered in the ellipsometry estimate of the thickness, and therefore to provide consistent results from our data the correct sample structure is $\mathrm{AlN_{film}/SiO_xN_y/Si_{subs}}$.

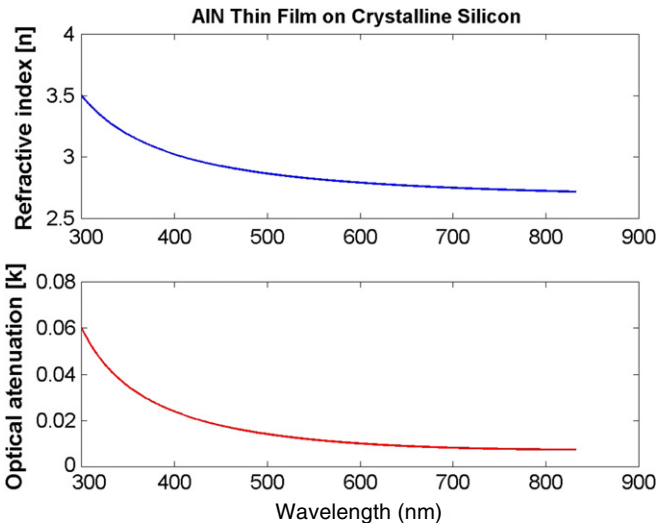

Figure 6. The top curve is the refractive index for AlN thin film on crystalline silicon, and the bottom curve is the corresponding optical attenuation.

4.3. Modified transmittance analysis

The modified optical analysis incorporating the interface layer was achieved by applying the well-known matrix theory for the two-layer system, in particular, the use of the corresponding Fresnel transmission coefficient (t) in the fashion of an Airy function and the transmittance, which is set as $T = (p_s/p_a)|t|^2$. Here p_s and p_a are the terms in the Airy function that describes t. The general details of these derivations can be found elsewhere in the literature [11].

This is used in our model together with the values of the refractive index and optical attenuation for crystalline silicon and those of the sub-layer (estimated to be silicon dioxide SiO_2), taken from the literature for both materials [14, 15]. Numerically, we simulate the thickness of the sub-layer by varying it in steps of 5 nm from zero to 400 nm to get the best fit to the experimental curve.

In figure 7(*a*), the solid line is the PATS-experimental data; the lower dashed curve is the calculated transmittance assuming the existence of a silicon oxide sub-layer. This was calculated using (14) with the results of the refractive index and optical attenuation displayed as the bottom curve in figure 6. The best fit corresponds to a sub-layer thickness of ∼230 nm, which is close to the value obtained from the analysis of the separation of the interference peaks given in section 4.1 ($n = 264.91 \pm 25$ nm). The difference might be due to the fact that the boundary between the film and the sub-layer is not abrupt. We include the uppermost curve (dotted line) which was the calculated transmittance of an AlN thin film monolayer of thickness: ∼265 nm; i.e. without the sub-layer. This curve is in good agreement with previous results; see, e.g., Kumar and Tansley [17].

The resulting PATS curves (solid lines), together with the transmittance curves, numerically reconstructed out of optical theory for AlN on quartz are displayed in figure 7(*b*). We display these for comparison only and to exhibit how well they replicate the optical spectra quality, a characteristic that was widely discussed in [1].

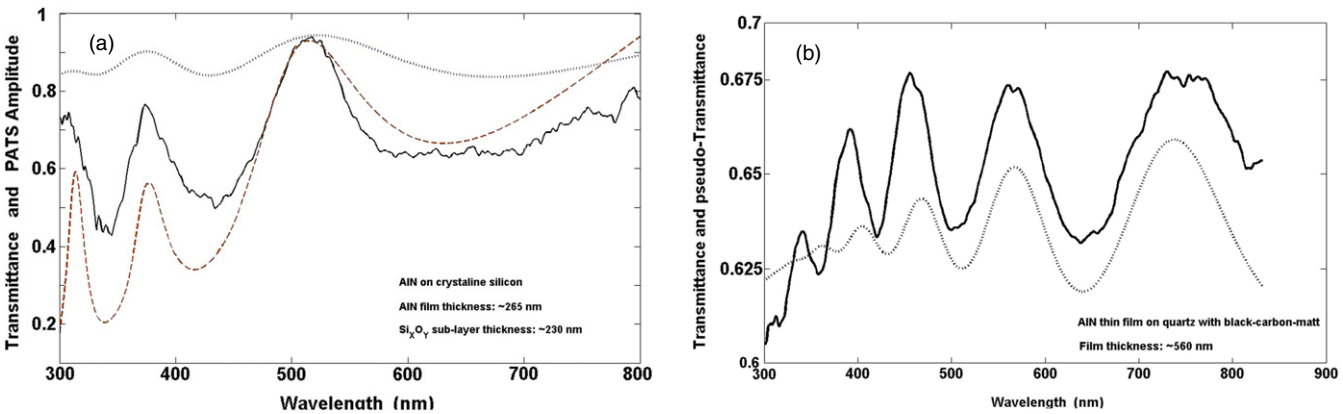

Figure 7. (*a*) The AlN thin film on crystalline silicon, the solid line is the PATS-experimental data, the upper dotted line is the calculated transmittance of the AlN thin film in air; and the lower dashed curve is the calculated transmittance on crystalline silicone substrate and assuming the type of sub-layer as indicated in section 4.2. (*b*) The PATS (solid line) and the calculated transmittance (dotted line) of the AlN thin film on quartz with carbon black.

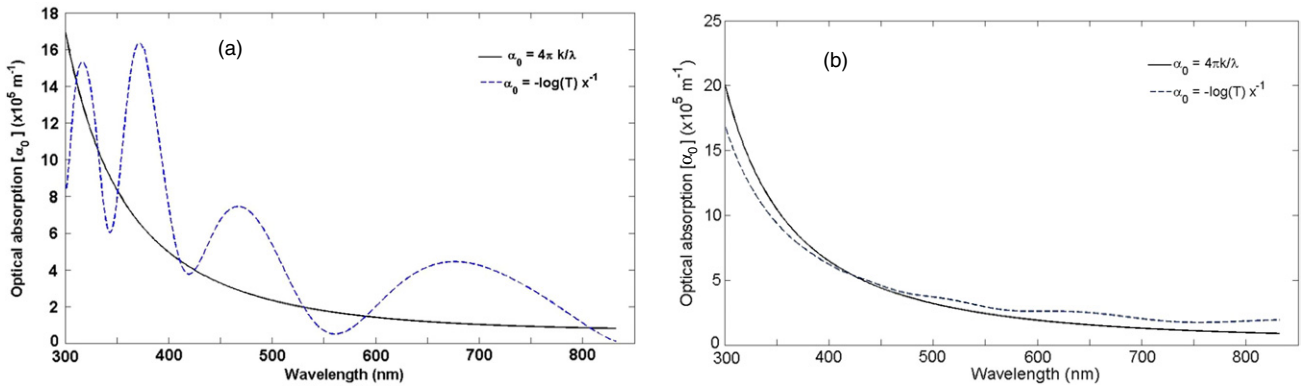

Figure 8. (*a*) and (*b*) are the optical absorption of AlN thin film on Si and quartz, respectively. The solid line is for calculating α_0 using optical dispersion theory; the dotted line is for α_0 calculated using Beer's law.

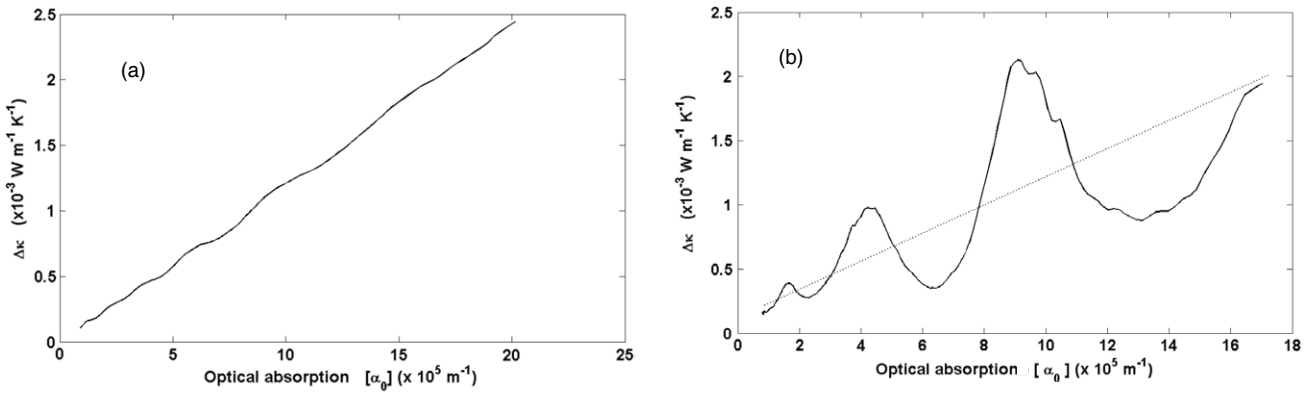

Figure 9. Thermal conductivity dispersion of AlN, against the optical absorption. This is for when the substrate is (*a*) quartz, and (*b*) crystalline silicon. The optical absorption was calculated from optical dispersion theory, where $k = 4\pi nd \sin\theta/\lambda$. In (*b*) the dotted line is a cartoon representation to suggest the tendency. The waving shape is inherent from the optical dispersion curves.

5. Thermal analysis

Previous analysis has shown that the thermal conductivity of AlN is comparable to that of various metals [18–20] making it an ideal candidate for the purpose of thermal analysis. As indicated in section 2, by taking the ratio of the raw data of the sample to the raw data of the substrate alone, it is possible to eliminate the thermal contributions from the substrate. It is known that silicon forms a natural oxide so that this substrate in fact has the structure of an oxide layer on top of the bulk of crystalline silicon [13, 19, 20]. Slack *et al* [21] identifies that at room temperature the highest value for thermal conductivity of pure AlN is 320 W m^{-1} K^{-1}. Other authors [22–24] report that the thermal conductivity values for polycrystalline AlN lie on the range 160–285 W m^{-1} K^{-1}, depending on the number of impurities (such as oxygen) and/or lattice defects. The thermal conductivity is directly related to the phonon mean-free-path (heat-carriers-free-path), which is determined by phonon–phonon scattering. Thus phonons propagate differently in each lattice, as a result of impurities or lattice defects; and where phonon scattering may occur. The phonon efficiency depends on how resonant is the coupling of the optical absorption with the lattice, being a function of the wavelength of illumination. Using the PATS curves and assuming $\kappa = 285$ W m^{-1} K^{-1}, we calculate the optical absorption curves for thin films of AlN on crystalline silicon and on quartz. In both cases we compare curves for α_0 calculated using Beer's law and also optical dispersion theory (with $\alpha_0 = 4\pi k/\lambda$, where the data for the extinction coefficient, $k = 4\pi nd \sin\theta/\lambda$, are those displayed in figures 5 and 6). The resulting curves are displayed in figure 8.

With this result at hand and using equation (6), we obtain the thermal conductivity variation within the experimental spectral range. The other parameters involved in (6) are the density and the specific heat. For our sample of AlN these are 3230 kg m^{-3} and 730 J kg^{-1} K^{-1}, respectively [9, 16, 18]. Then we calculate the thermal diffusivity of AlN, $a_{\mathrm{AlN}} = 1.209 \times 10^{-4}$ m^2 s^{-1}; and also the thermal diffusion coefficient, $\sigma = 624.397$ m^{-1}, this assuming our experimental modulation frequency of 15 Hz. We substitute these values in (6) and then we can obtain the thermal conductivity distribution, by taking Θ from the experimental PATS data and T from the Fresnel transmittance function; this last is obtained using the optical dispersion data displayed in figures 5 and 6. The resulting distribution is displayed in figures 9(*a*) and (*b*) for the deposit on crystalline silicon and quartz, respectively, and plotted against the optical absorption, whose values are obtained taking $\alpha_0 = 4\pi k/\lambda$, with $k = 4\pi nd \sin\theta/\lambda$. Furthermore,

the differences between the curves in figures 8(*a*), 8(*b*), 9(*a*) and 9(*b*) are because of the contributions from the SiO_xN_y sub-layer. The normalization process which was used to remove the instrumental and ambient effects does not remove the effect from the sub-layer since its thickness is not the same as that of the native oxide, as can be seen from the curve in figure 7(*a*). Still, in both cases we present here, the average thermal conductivity value is within the range of values already reported in the literature [9, 21–24]. The difference in the value of the thermal conductivity, in the two examples we present, is well explained by the presence of oxygen as impurity.

The curves in figures 9 were normalized to the environment temperature (∼300 K). From the former set we observe that the increase in variation of κ goes almost linear with the increase in the optical absorption. Equally for low optical absorption rate, the change in κ is also comparatively small. From this analysis and as displayed in equation (6), it seems that there is a linear relationship between the optical absorption and the thermal conductivity. The existence of relationships between the optical field and the thermal properties is nothing new. The most apparent prior example is the so-called Widemann–Franz law: that is, the ratio of the thermal conductivity to the electric conductivity is proportional to the temperature change multiplied by a constant, called Lorenz's constant. At first sight, the curves in figure 9 suggest a relationship of that kind; however, at this point it is too early to confirm it. Confirmation of the existence of such a relationship is a major task, and thus out of the scope of the current work.

6. Conclusions

Our results demonstrate that the PATS technique using a single set of spectroscopic measurements can be used to derive both the optical and photothermal properties of thin films. The results are in good agreement with previous results dedicated to the optical or thermal analysis of thin films [14, 18, 21]. In this paper we have used the PATS technique to perform the analysis of a single layer; however, there appears to be no experimental or theoretical limitation to prohibit the extension of the present model to analyse multilayer samples.

The interaction of radiation with matter always involves, in one way or other, radiative and non-radiative processes, and in the latter case thermal processes are always involved. Therefore, the possibility for the simultaneous analysis of the thermal and optical properties is not restricted by the instrument; this capability results from material properties and the efficacy to produce photothermal waves, as described in section 3. The actual representation of this efficacy is given in equation (9), which is a measure of the efficiency of the transference of optical to thermal energy. Since the case we present here is just an arbitrary example, as displayed in figure 9, this invites us to ask if there exists a more fundamental relationship between the optical and thermal properties. That is, does there exist a general relationship similar to the Widemann–Franz law for metals, for all materials including dielectrics and semiconductors? If so, then it would act as a description of the transformation of energy from the thermal to the optical domain, and vice versa.

From figure 7 it is apparent that the current method provides reliable quantitative information related to the optical properties of a monolayer thin film system, regardless of the optical transparency of the substrate. Simultaneously, it is possible to obtain reliable quantitative results related to the thermal conductivity, figure 8, and the ratio of the thermal diffusivity to the optical attenuation as expressed by equation (9) and displayed in figure 9. The average values for AlN are in agreement with the literature [21]. Similarly, it appears that equation (9) can be taken to express the effective efficiency of the energy transfer between the optical and the thermal processes. However, this last idea is a first approach that requires further analytical consideration.

Acknowledgments

CGS wants to thank J-P Connerade at the Physics Department of Imperial College, London, for the fruitful discussions related to this article; he also wants to thank the WIPM-CAS in China for the support and permission to dedicate valuable time to this work over the academic period working with them. This work was partially supported by DGAPA at the Universidad Nacional Autonónoma de México and the Consejo Nacional de Ciencia y Tecnología (CONACyT, México) via the grants IN100706 and P47758212, respectively.

References

[1] García-Segundo C, Villagrán-Muniz M and Muhl S 1998 Determination of thin film optical properties by the photoacoustic OPC technique *J. Phys. D: Appl. Phys.* **31** 165–71
[2] Charpentier P, Lepoutre F and Bertrand L 1982 Photoacoustic measurements of thermal diffusivity description of the drum effect *J. Appl. Phys.* **53** 608–14
[3] Rosencwaig A and Gersho A 1976 Theory of the photoacoustic effect with solids *J. Appl. Phys.* **47** 64–9
[4] McDonald F A and Wetsel G C Jr 1978 Generalized theory of the photoacoustic effect *J. Appl. Phys.* **49** 2313–22
[5] Tam A C 1986 Applications of photoacoustic sensing techniques *Rev. Mod. Phys.* **58** 381–431
[6] Marquezini M V, Cella N, Mansanares A M, Vargas H and Miranda L C M 1991 Open photoacoustic cell spectroscopy *Meas. Sci. Technol.* **2** 396–401
[7] Mansanares A M, Vargas H, Galembeck F, Buijs J and Bicanic D 1991 Photoacoustic characterization of a two-layer system *J. Appl. Phys.* **70** 7046–50
Mansanares A M, Bento A C, Vargas H, Leite N F and Miranda L C M 1990 *Phys. Rev.* B **42** 4477–86
[8] Garcia-Segundo C, Smith A J and Connerade J-P 2004 Optically induced non-radiative fast pulses in metals *J. Mod. Opt.* **51** 233–53
[9] Harima H 2002 *J. Phys.: Condens. Matter* **14** R967–93
[10] Shankes H R, Maycock P D, Sidles P H and Danielson G C 1963 *Phys. Rev.* **130** 1743–8
[11] Born M and Wolf E 1980 *Principles of Optics* (London: Pergamon)
[12] Andrievskii B V, Vakhuovich V F, Kurlyak V Yu and Romanyuk N A 1988 *Opt. Spectrosc. USSR* **65** 79
[13] Hass G and Salzberg C D 1954 *J. Opt. Soc. Am.* **44** 181–7
[14] Brunner D *et al* 1997 *J. Appl. Phys.* **82** 5090–6
[15] Philipp H R and Taft E A 1954 *Phys. Rev.* **120** 37–8
[16] Palik E D 1985 *Handbook of Optical Constants of Solids* (New York: Academic)

[17] Kumar S and Tansley T L 1995 *Japan. J. Appl. Phys.* **34** 4154–8
[18] Nipko J C and Loong C-K 1998 *Phys. Rev.* B **57** 10550–4
[19] Laughlin R B 1980 *Phys Rev.* B **22** 3021–9
[20] Deal B E and Grive A S 1963 *J. Appl. Phys.* **36** 3770–8
[21] Slack G A, Tanzilli R R, Pohl R O and Vandersande J W 1987 The intrinsic thermal conductivity of AlN *J. Phys. Chem. Solids* **48** 641–7
[22] Jarrige J, Lecompte J P, Mullot J and Miille G 1997 Effect of oxygen on the thermal conductivity of AlN ceramics *J. Eur. Ceram. Soc.* **17** 1891
[23] Harris J H, Youngman R A and Teller R G 1990 On the nature of the oxygen-related defect in aluminum nitride *J. Meas. Res.* **5** 1763
[24] Pandey D K and Yadav R R 2009 Temperature dependent ultrasonic properties of aluminium nitride *Appl. Acoust.* **70** 412–5
[25] Yamaguchi S, Izaki R, Yamagiwa K, Taki K and Iwamura Y 2003 Thermal diffusivity and thermoelectric figure of merit of $Al_{1-x}In_xN$ prepared by reactive radio-frequency sputtering *Appl. Phys. Lett.* **83** 5398–400